COMPARING DIFFERENT APPROACHES FOR MODELING THE VERTICAL MOTION OF THE EC 135

Susanne Seher-Weiss
German Aerospace Center (DLR), Institute of Flight Systems
Lilienthalplatz 7, 38108 Braunschweig, Germany
susanne.seher-weiss@dlr.de

ABSTRACT

Helicopters like the EC 135 with its bearingless main rotor design feature large equivalent hinge offsets of about 10 %, significantly higher than conventional rotor designs and leading to improved maneuverability and agility. For such a helicopter, the fuselage and rotor responses become fully coupled and the quasi-steady assumption using a 6-DoF rigid-body model state space description and approximating the neglected rotor degrees of freedom by equivalent time delays is not suitable. Depending on the intended use of the model, the accurate mathematical description of the vertical motion for these configurations requires an extended model structure that includes inflow and coning dynamics. The paper first presents different modeling approaches and their relationship. Next, identification results for the DLR EC 135 are presented for a model that only describes the vertical motion excluding coupling to the other axes. Here, the differences between the modeling approaches and the respective deficits are explained. Next, the modelling approach most widely used in the rotorcraft identification literature is extended to account for hinge offset. In addition, some model parameters are estimated instead of fixing them at their theoretical predictions which leads to a very good match with EC 135 flight test data. Results for a complete model of the EC 135 including flapping, coning/inflow, and regressive lead-lag are shown as a final result.

NOMENCLATURE

a_z	vertical acceleration, m/s^2
B_i	coning derivatives (i = ν, β_0, $\dot{\beta}_0$, δ_{col})
c	rotor blade chord, m
C_{L_α}	blade lift curve slope, 1/rad
C_T	thrust coefficient, $C_T = T/[\rho\pi R^2(\Omega R)^2]$
C_0	inflow constant
e	hinge offset, m
g	acceleration due to gravity, m/s^2
I_β	blade flapping moment of inertia, kg m^2
K_β	flapping stiffness, Nm/Rad
K_{θ_0}	control gain, rad/%
m	aircraft mass, kg
p, q, r	roll, pitch and yaw rates, rad/s
R	rotor radius, m
s	Laplace variable, 1/s
T	rotor thrust, N
T_i	thrust derivatives (i = ν, $\dot{\nu}$, $\dot{\beta}_0$)
u, v, w	body-fixed velocity components, m/s
V_i	inflow derivatives (i = ν, $\dot{\nu}$, $\dot{\beta}_0$)
Z_i	vertical force derivatives (i = u, v, w, p, q, r, ν, $\dot{\beta}_0$, C_T, δ_{lon}, δ_{lat}, δ_{ped}, δ_{col})
β_0	coning angle, rad
δ_{lon}, δ_{lat}	longitudinal, lateral cyclic inputs, %
δ_{ped}, δ_{col}	pedal and collective inputs, %
ϵ	hinge offset ratio, $\epsilon = e/R$
Φ, Θ	roll and pitch angles, rad
γ	Lock number, $\gamma = \rho C_{L_\alpha} c R^4 / I_\beta$
ν	inflow, m/s
$\bar{\nu}_0$	trim inflow ratio
ρ	air density, kg/m^3
σ	solidity
τ	time delay, s
Ω	rotor rotation speed, rad/s

Subscripts

m	measured value
0	trim value

Within the differential equations, all state variables (w, ν, β_0) as well as all control inputs (δ_{lon}, δ_{lat}, δ_{ped}, δ_{col}) denote perturbations from trim.

1. INTRODUCTION

High-bandwidth flight control system development requires linear models with good fidelity over a wide frequency range. Such models can be derived by linearization of a full flight envelope nonlinear simulation model or by system identification. When appropriate flight test data are available, system identification usually yields more accurate models than linearization.

Helicopter system identification for flight control system development often requires models with a high number of states because of the high degree of inter-axis coupling and the need to represent the main rotor degrees of freedom. Especially when a model with a large frequency range of validity is desired, an extended model structure is necessary that explicitly includes the regressive flapping, coupled inflow/coning, and regressive lead-lag states of the rotor.

Regarding the vertical axis, a quasi-static model is therefore usually not sufficient. An implicit model formulation that includes dynamic inflow and accounts for coning through an equivalent time delay was presented in[1] and successfully applied to DLR EC 135 data in forward flight. This implicit formulation is equivalent to the approach presented in[2] for the identification of the AH-64, where the dynamic inflow is approximated by a first order lead-lag filter in the collective term in the vertical axis.

For modeling the coupling between the fuselage and the inflow/coning dynamics, the approach most widely used is the hybrid formulation developed by Tischler[3]. It is based on the analytical model for the coupled inflow/coning/heave dynamics from Chen/Hindson[4]. The hybrid model uses a simplified version of the model from[4] that ignores heave motion and the influence of hinge offset. The coning dynamics are expressed by a second-order differential equation that is coupled to the first order equation for inflow. These inflow/coning dynamics are then coupled to the fuselage through the perturbation thrust coefficient. The hybrid model approach has been successfully applied for identification of the vertical motion of the S-92[5], SH-2G[6], AH-64D[7] and S-76C[8].

As blade motion (including coning), inflow, and thrust measurements are usually not available, most parameters of this hybrid model are normally fixed to theoretical values. In[9] Fletcher identified some of the parameters of the hybrid model for the UH-60.

Figure 1: DLR's research helicopter ACT/FHS

The DLR Institute of Flight Systems operates the ACT/FHS (Active Control Technology/Flying Helicopter Simulator, see figure 1), an EC 135 helicopter with a highly modified flight control system[10]. To support the in-flight simulation efforts, models for the EC 135 helicopter that cover the envelope from hover up to 120 kts forward flight have to be identified. Dedicated flight tests for this purpose, consisting of frequency sweeps and multistep inputs in all four controls, have been performed at five reference speeds. Within this modeling effort, different modeling variants are currently under investigation[11]. Therefore, different approaches for modeling the vertical motion were investigated using EC 135 flight test data.

2. MODELING OF THE VERTICAL AXIS

The vertical response to collective input at low frequencies (below 1 rad/s) is dominated by the first-order helicopter heave damping caracteristic. At mid to high frequencies (about 1-12 rad/s), the vertical response is characterized by the coupled inflow/coning dynamics. At higher frequencies, the response is dominated by the second-order coning dynamics with a natural frequency of about 1/rev (the exact frequency depends on hinge offset and flapping stiffness).

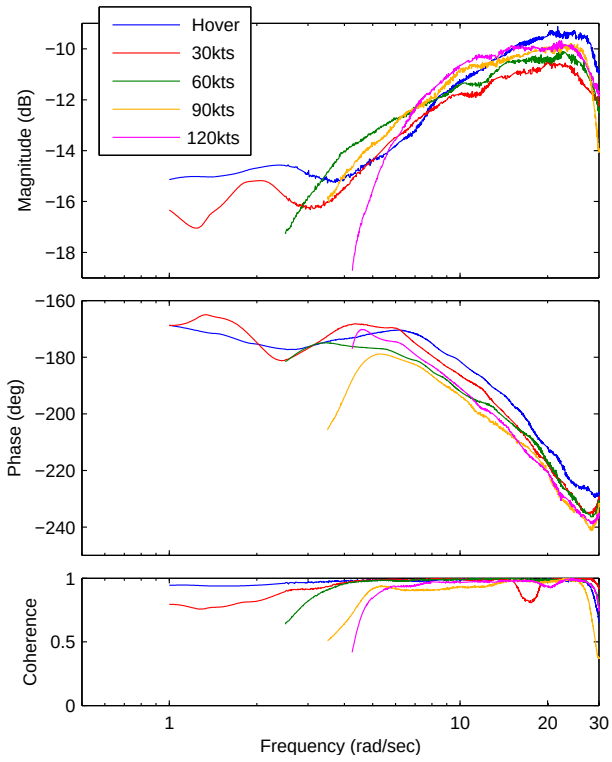

Figure 2: Measured frequency responses for a_z/δ_0 (EC 135 data)

The frequency responses for vertical acceleration due to collective pilot control input as derived from EC 135 flight test data are depicted in figure 2. For frequencies greater that 30 rad/s the coherence drops drastically so that the data is no longer reliable and thus not shown. It can be seen, that neither the amplitude nor the phase curves are flat, not even in forward flight where a simple quasi-static model is often assumed to be sufficient.

2.1 Quasi-Static Model

The quasi-static formulation assumes that the inflow and coning reach their steady state instantaneously upon a collective control input. The vertical response is thus described

by the first-order equation

$$\dot{w} = Z_w w + Z_{\delta_{col}} \delta_{col} \tag{1}$$

The the two derivatives Z_w and $Z_{\delta_{col}}$ are usually estimated but theoretical predictions of

$$\begin{aligned} Z_w &= \frac{\rho C_{L_\alpha} \sigma \Omega R}{8m/(\pi R^2)(1 + C_{L_\alpha}\sigma/(16\bar{\nu}_0))} \\ Z_{\delta_{col}} &= -\frac{4}{3}\Omega R Z_w \end{aligned} \tag{2}$$

with $\bar{\nu}_0 = \sqrt{T_0/(\rho\pi R^2(\Omega R)^2)}$ exist (see[4]).

Assuming $a_z = \dot{w}$, this yields a transfer function of

$$\frac{a_z}{\delta_{col}} = \frac{s Z_{\delta_0}}{s - Z_w} \tag{3}$$

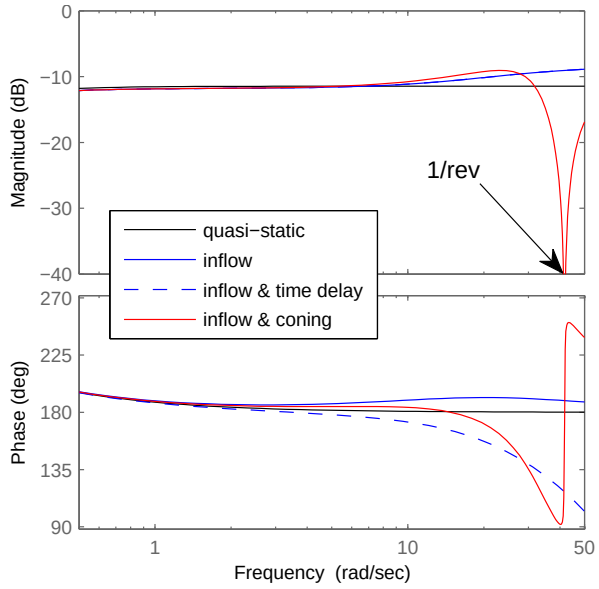

Figure 3: Simulated frequency responses for a_z/δ_0 using different models (EC 135 in hover)

Parameter	Value	
c	0.29	m
C_{L_α}	5.6	1/rad
e	0.507	m
I_β	204.16	kg m^2
K_β	-4855	Nm/rad
K_{θ_0}	0.00302	rad/%
m	2110	kg
R	5.1	m
T_0	28000	N
γ	7.35	
ρ	1.225	kg/m^3
σ	0.0724	
Ω	41.36	rad/s

Table 1: Values for the EC 135 configuration parameters

The first curve in figure 3 is a simulation of the transfer function from equation (3) with the predictions from equation (2) and values from table 1. It can be seen that the quasi-static formulation leads to flat amplitude and phase curves at higher frequencies for vertical acceleration due to collective control.

Comparing this frequency response to the experimental data from figure 2 clearly shows that quasi-static modeling of the vertical axis is not sufficient. Therefore, the influence of inflow and coning must be taken into account if the identified models are to be accurate at higher frequencies.

2.2 Accounting for Inflow

An implicit model that includes the first order inflow equation and accounts for coning through an equivalent time delay was derived in[1] as follows. The dynamic equations for vertical velocity w and inflow ν for a rigid rotor (neglecting coning) are

$$\begin{aligned} \dot{w} &= Z_w w + Z_\nu \nu + Z_{\dot{\nu}} \dot{\nu} \\ \dot{\nu} &= T_w w + T_\nu \nu + T_{\delta_{col}} \delta_{col} \end{aligned} \tag{4}$$

The second equation from above, the inflow equation, is derived from the principle of linear momentum. Inserting it into the first equation eliminates $\dot{\nu}$ and leads to

$$\begin{aligned} \dot{w} &= (Z_w + Z_{\dot{\nu}} T_w) w + (Z_\nu + Z_{\dot{\nu}} T_\nu)\nu \\ &\quad + Z_{\dot{\nu}} T_{\delta_{col}} \delta_{col} \\ &= \bar{Z}_w w + \bar{Z}_\nu \nu + \bar{Z}_{\delta_{col}} \delta_{col} \end{aligned} \tag{5}$$

Solving this equation for ν yields

$$\nu = (\dot{w} - \bar{Z}_w w - \bar{Z}_{\delta_{col}} \delta_{col})/\bar{Z}_\nu \tag{6}$$

Differentiating equation (5) with respect to time and inserting the expressions for $\dot{\nu}$ from (4) and for ν from (6) gives

$$\begin{aligned} \ddot{w} &= (\bar{Z}_\nu T_w - T_\nu \bar{Z}_w) w + (\bar{Z}_w + T_\nu)\dot{w} \\ &\quad + (\bar{Z}_\nu T_{\delta_{col}} - T_\nu \bar{Z}_{\delta_{col}})\delta_{col} + \bar{Z}_{\dot{\delta}_{col}} \dot{\delta}_{col} \\ &= \hat{Z}_w w + \hat{Z}_{\dot{w}} \dot{w} + \hat{Z}_{\delta_{col}} \delta_{col} + \hat{Z}_{\dot{\delta}_{col}} \dot{\delta}_{col} \end{aligned} \tag{7}$$

This differential equation for $\ddot{w}$ has both the collective control input δ_{col} and its derivative $\dot{\delta}_{col}$ as inputs. Alternatively, δ_{col} can be added to the model as a state variable, which then leaves $\dot{\delta}_{col}$ as the only vertical control input.

Again assuming $a_z = \dot{w}$ yields the transfer function

$$\frac{a_z}{\delta_{col}} = \frac{s(\hat{Z}_{\dot{\delta}_{col}} s + \hat{Z}_{\delta_{col}})}{s^2 - \hat{Z}_{\dot{w}} s - \hat{Z}_w} \tag{8}$$

The second curve in figure 3 is a simulation of the transfer function from equation (8) with numerical values according to equation (25). It shows that accounting only for inflow

and not for coning leads to a rising amplitude in the vertical response at higher frequencies but yields no phase reduction. The third curve in the figure illustrates that the phase drop that is caused by the coning can approximately be accounted for if the implicit model from equation (8) is extended by an equivalent time delay.

In[2], Schroeder et. al. presented a modeling approach that uses a first order lead-lag filter on the vertical control input to account for inflow.

$$\begin{aligned} \dot{w} &= Z_w w + Z_{\delta_{col}} \delta_{col_{LL}} \\ \text{with} \quad \delta_{col_{LL}} &= \frac{s+a}{s+b} e^{-\tau_{col} s} \delta_{col} \end{aligned} \tag{9}$$

The zero a and pole b of the lead-lag filter as well as the time delay τ_{col} and the derivatives Z_w and $Z_{\delta_{col}}$ were estimated from flight test data.

Deriving the transfer function from collective input to vertical velocity for this model

$$\frac{w}{\delta_{col}} = \frac{Z_{\delta_{col}} s + Z_{\delta_{col}} a}{s^2 - (Z_w - b)s - Z_w b} e^{-\tau_{col} s} \tag{10}$$

illustrates that this approach is equivalent to the implicit formulation from equation (8) with

$$\begin{aligned} \hat{Z}_{\dot{w}} &= Z_w - b, & \hat{Z}_w &= Z_w b, \\ \hat{Z}_{\dot{\delta}_{col}} &= Z_{\delta_{col}}, & \hat{Z}_{\delta_{col}} &= Z_{\delta_{col}} a \end{aligned} \tag{11}$$

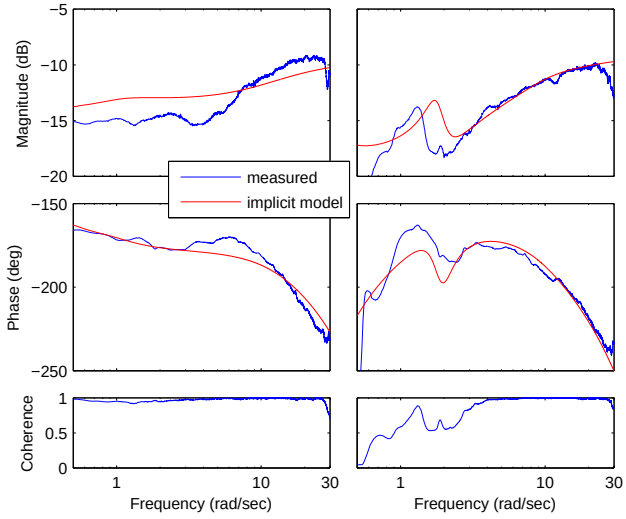

Figure 4: Match in a_z/δ_0 for the implicit model in hover (left) and at 60 kts forward flight (right) (EC 135 data)

The implicit formulation from equation (7) was included in an 11-DoF model and applied to EC 135 data[1]. Figure 4 shows that this model that accounts only for inflow and not explicitely for coning is sufficient for forward flight but is not able to match the hover flight test data.

2.3 Coupled Inflow/Coning Equations

Tischler[3] developed a hybrid model that couples the inflow/coning dynamics with the fuselage. It is based on the work by Chen and Hindson[4] who developed analytical models for the coupled inflow/coning/heave dynamics. By ignoring the aircraft heave motion, a very simple physical model of the coupled inflow/coning response is obtained that is quite accurate at mid and high frequencies (above 1 rad/s).

The first-order inflow dynamics equation are written as

$$\begin{aligned} \dot{\nu} =& \frac{-75\pi\Omega}{32}\left(\bar{\nu}_0 + \frac{C_{L\alpha}\sigma}{16}\right) C_0 \nu + V_{\dot{\beta}_0}\dot{\beta}_0 \\ &+ \frac{25\pi\Omega^2 R}{32}\left(\frac{C_{L\alpha}\sigma}{8}\right) C_0 K_{\theta_0}\delta_{col} \\ =& V_\nu \nu + V_{\dot{\beta}_0}\dot{\beta}_0 + V_{\delta_{col}}\delta_{col} \end{aligned} \tag{12}$$

where the trim inflow ratio $\bar{\nu}_0$ and thrust coefficient C_{T_0} are defined as ($T_0 = mg$)

$$\bar{\nu}_0 = \sqrt{\frac{C_{T_0}}{2}}, \qquad C_{T_0} = \frac{T_0}{\rho\pi R^2 (\Omega R)^2} \tag{13}$$

The control gain K_{θ_0} transforms collective input to effective blade root pitch angle (θ_0). For hovering flight, an analytical expression is available for $V_{\dot{\beta}_0}$

$$V_{\dot{\beta}_0} = \frac{-25\pi\Omega R}{32}\left(\bar{\nu}_0 + \frac{C_{L\alpha}\sigma}{8}\right) \tag{14}$$

The rigid-blade coning dynamics, ignoring the influence of hinge offset and flapping spring, are expressed as a second-order differential equation

$$\begin{aligned} \ddot{\beta}_0 =& -\frac{\Omega\gamma}{8}\dot{\beta}_0 - \Omega^2\beta_0 - \frac{\Omega\gamma}{6R}\nu + \frac{\Omega^2\gamma}{8}K_{\theta_0}\delta_{col} \\ =& B_{\dot{\beta}_0}\dot{\beta}_0 + B_{\beta_0\beta_0} + B_\nu \nu + B_{\delta_{col}}\delta_{col} \end{aligned} \tag{15}$$

resulting in two states, coning angle β_0 and coning rate $\dot{\beta}_0$.

Finally, the coning/inflow dynamics are coupled to the fuselage through the thrust coefficient C_T, to achieve the hybrid model structure for the vertical dynamics

$$\begin{aligned} \dot{w} =& Z_u u + Z_v v + Z_w w + (Z_p - v_0)p \\ &+ (Z_q + u_0)q + Z_r r - g\cos\Phi_0 \sin\Theta_0 \Theta \\ &- \frac{\rho\pi R^2 (\Omega R)^2}{m} C_T + Z_{\delta_{lon}}\delta_{lon} + Z_{\delta_{lat}}\delta_{lat} \\ &+ Z_{\delta_{ped}}\delta_{ped} \end{aligned} \tag{16}$$

where the perturbation thrust coefficient C_T is given by

$$\begin{aligned} C_T =& \frac{0.543}{\Omega^2 R}\frac{1}{C_0}\dot{\nu} + \frac{4\bar{\nu}_0}{\Omega R}\nu + \frac{4\bar{\nu}_0}{3\Omega}\dot{\beta}_0 \\ =& T_{\dot{\nu}}\dot{\nu} + T_\nu \nu + T_{\dot{\beta}_0}\dot{\beta}_0 \end{aligned} \tag{17}$$

Note that the quasi-steady collective control force derivative $Z_{\delta_{col}}$ is absent from equation (16) for the vertical acceleration because the control path is now extended. Collective control inputs cause an increase in blade angle of attack that increases inflow and coning (see equations (12) and (15)). The corresponding dynamic variations in thrust from equation (17) are transmitted to the fuselage via equation (16) resulting in a change of vertical acceleration.

The fourth curve in figure 3 is the simulated vertical acceleration responses that is obtained with equations (12) – (15) using a value of $C_0 = 1$ and a simplified version of equation (16) that omits all coupling with the off-axis states (u, v, p, q, r) and the secondary inputs (δ_{lon}, δ_{lat}, δ_{ped}). It can be seen that the hybrid model with inflow and coning leads to a transfer function zero at the rotor frequency.

As introduced by Chen[4], the inflow constant C_0 in equations (12) and (17) allows for the selection of either the Carpenter-Fridovich theory inflow time constant ($C_0 = 0.639$) or the Pitt-Peters time constant ($C_0 = 1$).

Carpenter[12] extended the simple momentum theory for steady-state inflow to include the transient inflow buildup by introducing the apparent additional mass of air m_a participating in the acceleration. By analogy with an impervious disk, Carpenter defined the apparent additional mass to be 63.7% of the air mass of the sphere circumscribed by the rotor ($m_a = 0.637\rho\frac{4}{3}\pi R^3$). Taking the equation for the instantaneous thrust

$$T = m_a\dot{\nu} + 2\pi R^2\rho\nu\left(\nu - w + \frac{2}{3}\dot{\beta}_0 R\right) \tag{18}$$

and taking into account that $C_T = T/(\rho\pi R^2(\Omega R)^2)$ the first term in equation (17) becomes

$$\frac{m_a}{\rho\pi R^2(\Omega R)^2}\dot{\nu} \approx 0.849\frac{\dot{\nu}}{\Omega^2 R} \tag{19}$$

The Pitt-Peters dynamic inflow model from[13] was developed based on unsteady actuator disk theory. Closed-form formulae were obtained that relate transient rotor thrust and pitch and roll moments to the transient response of the rotor-induced flow field. The corresponding equation for the first term in equation (17) for this model is

$$\frac{128}{75\pi\Omega}\frac{\dot{\nu}}{\Omega R} \approx 0.543\frac{\dot{\nu}}{\Omega^2 R} \tag{20}$$

This means that the Pitt-Peters model has a smaller apparent additional air mass (about 64 % of the value for the Carpenter-Fridovich model) resulting in a smaller time constant of the inflow mode.

Figure 5 shows the difference between the vertical acceleration responses for both inflow models. It can be seen that

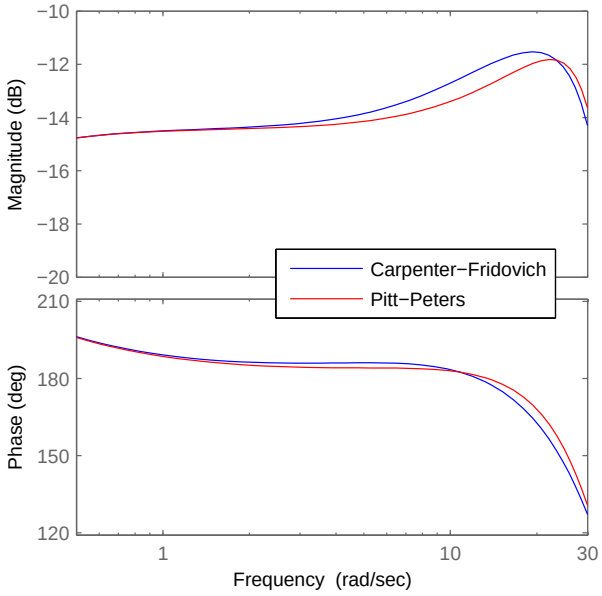

Figure 5: Simulated response of a_z/δ_0: Comparison between Carpenter-Fridovich and Pitt-Peters inflow model

for the Carpenter-Fridovich model the amplitude raise starts at lower frequencies compared to the Pitt-Peters theory and that the maximum amplitude is higher.

Most system identification performed using the hybrid formulation uses the Carpenter-Fridovich model[6]. Due to the lack of blade motion, inflow and thrust measurements, all derivatives of the inflow and coning equations are usually fixed at their theoretical predictions and only Z_w is estimated.

2.4 Relationship between the Formulations

Tischler[3] implements equation (17) by introducing a fictitious state derivative and formulating the system dynamics using a mass matrix. Alternatively, all equations of the vertical axis can be solved for the state derivatives and written in standard matrix notation. Writing equations (12) and (15) in matrix notation yields

$$\begin{pmatrix}\dot{\nu}\\ \dot{\beta}_0\\ \ddot{\beta}_0\end{pmatrix} = \begin{bmatrix}V_\nu & 0 & V_{\dot{\beta}_0}\\ 0 & 0 & 1\\ B_\nu & B_{\beta_0} & B_{\dot{\beta}_0}\end{bmatrix}\begin{pmatrix}\nu\\ \beta_0\\ \dot{\beta}_0\end{pmatrix} + \begin{bmatrix}V_{\delta_{col}}\\ 0\\ B_{\delta_{col}}\end{bmatrix}\delta_{col} \tag{21}$$

To be able to write equation (16) also in matrix notation, equation (17) must be used for the perturbation thrust coefficient and $\dot{\nu}$ from equation (12) inserted. This finally yields

$$\begin{aligned}\dot{w} =& Z_u u + Z_v v + Z_w w + (Z_p - v_0)p\\ &+ (Z_q + u_0)q + Z_r r - g\cos\Phi_0\sin\Theta_0\Theta\\ &+ Z_\nu\nu + Z_{\dot{\beta}_0}\dot{\beta}_0 + Z_{\delta_{col}}\delta_{col}\\ &+ Z_{\delta_{lon}}\delta_{lon} + Z_{\delta_{lat}}\delta_{lat} + Z_{\delta_{ped}}\delta_{ped}\end{aligned} \tag{22}$$

with

$$
\begin{aligned}
Z_\nu &= Z_{C_T}(T_{\dot\nu} V_\nu + T_\nu),\\
Z_{\dot\beta_0} &= Z_{C_T}(T_{\dot\nu} V_{\dot\beta_0} + T_{\dot\beta_0}),\\
Z_{\delta_{col}} &= Z_{C_T} T_{\dot\nu} V_{\delta_{col}},\\
Z_{C_T} &= -\frac{\rho\pi R^2(\Omega R)^2}{m}
\end{aligned}
\tag{23}
$$

To be able to compare the hybrid model with the implicit formulation, the preceding equations are reduced to the case of inflow only by setting $\dot\beta_0 = \beta_0 = 0$ in equations (21) and (22) and omitting all coupling terms in equation (22). This yields

$$
\begin{aligned}
\dot\nu &= V_\nu \nu + V_{\delta_{col}} \delta_{col}\\
\dot w &= Z_w w + Z_\nu \nu + Z_{\delta_{col}} \delta_{col}
\end{aligned}
\tag{24}
$$

Differentiating the second equation from above with respect to time and inserting $\dot\nu$ from the first and ν from the second equation yields the implicit formulation from equation (7) with

$$
\begin{aligned}
\hat Z_w &= -Z_w V_\nu\\
\hat Z_{\dot w} &= Z_w + V_\nu\\
\hat Z_{\dot\delta_{col}} &= Z_\nu V_{\delta_{col}} - V_\nu Z_{\delta_{col}}\\
\hat Z_{\delta_{col}} &= Z_{\delta_{col}}
\end{aligned}
\tag{25}
$$

Inserting the analytical values for V_ν and $V_{\delta_{col}}$ from equation (12) as well as the expressions for Z_ν and $Z_{\delta_{col}}$ from equation (23) leads to

$$
\begin{aligned}
\frac{\hat Z_{\dot\delta_{col}}}{\hat Z_{\delta_{col}}} &= \frac{T_{\dot\nu}}{T_\nu} = \frac{1}{C_0}\frac{0.543}{4\Omega\bar\nu_0}\\
\hat Z_{\dot w} &= Z_w + \frac{-75\pi\Omega}{32}\left(\bar\nu_0 + \frac{C_{L\alpha}\sigma}{16}\right) C_0\\
\hat Z_w &= \frac{75\pi\Omega}{32}\left(\bar\nu_0 + \frac{C_{L\alpha}\sigma}{16}\right) C_0 Z_w
\end{aligned}
\tag{26}
$$

The first equation shows that the two control derivatives $\hat Z_{\delta_{col}}$ and $\hat Z_{\dot\delta_{col}}$ from the implicit model are proportional to each other with a factor that depends on the inflow constant C_0. Furthermore, the parameters $\hat Z_w$ and $\hat Z_{\dot w}$ are also not independent but are coupled via V_ν and are both a function of Z_w, that is usually estimated.

For the EC 135, inserting the values from table 1 into equation (26) and using the Carpenter-Fridovich value for C_0 results in a proportionality between the two control derivatives of $\hat Z_{\dot\delta_{col}} = 0.0916 \hat Z_{\delta_{col}}$. This restriction was utilized throughout the identification with the implicit model. The dependency between $\hat Z_w$ and $\hat Z_{\dot w}$ was ignored at first which led to correlation problems in the identification, especially in the hover and low speed regime. Therefore, these two derivatives were coupled (via V_ν, see equation (25)) for the final identification.

2.5 Application to EC 135 Data

To investigate whether the hybrid model from section 2.3 would yield an improvement over the implicit formulation, the following reduced model, that covers only the vertical axis, was used. This approach is appropriate for the hover flight condition where the vertial axis dynamics should be relatively decoupled from the rest of the model.

$$
\begin{pmatrix} \dot w\\ \dot\nu\\ \dot\beta_0\\ \ddot\beta_0 \end{pmatrix} =
\begin{bmatrix} Z_w & Z_\nu & 0 & Z_{\dot\beta_0}\\ 0 & V_\nu & 0 & V_{\dot\beta_0}\\ 0 & 0 & 0 & 1\\ 0 & B_\nu & B_{\beta_0} & B_{\dot\beta_0} \end{bmatrix}
\begin{pmatrix} w\\ \nu\\ \beta_0\\ \dot\beta_0 \end{pmatrix} +
\begin{bmatrix} Z_{\delta_{col}}\\ V_{\delta_{col}}\\ 0\\ B_{\delta_{col}} \end{bmatrix} \delta_{col}
\tag{27}
$$

In this model, all parameters of the coning equation are known. In the inflow equation, $V_{\dot\beta_0}$ is known from equation (14) and V_ν and $V_{\delta_{col}}$ are determined according to equation (12). A value of 0.639 was chosen for the inflow constant C_0 which corresponds to the Carpenter-Fridovich theory. In the heave equation, Z_w is a free parameter whereas Z_ν, $Z_{\dot\beta_0}$ and Z_{δ_0} are determined according to equation (23).

The unknown parameters of this reduced model, that have to be estimated, are thus Z_w and a time delay $\tau_{\delta_{col}}$ that is necessary to account for internal dynamics of the control system.

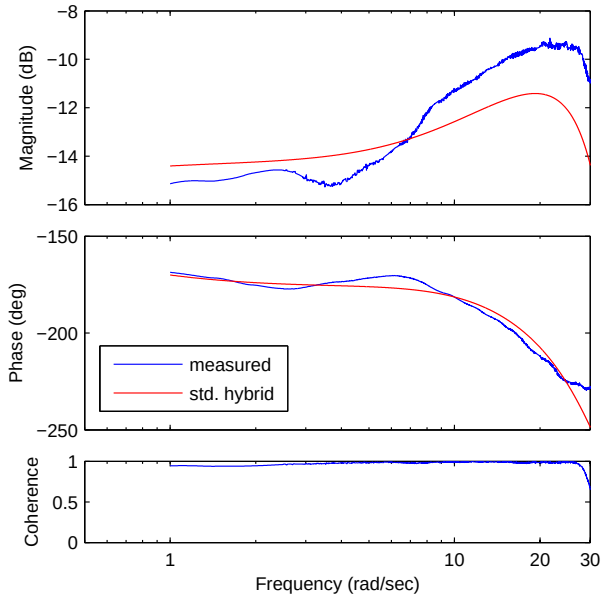

Figure 6: Match in a_z/δ_0 for the standard hybrid model (EC 135 in hover)

Figure 6 illustrates that accounting for coning with the standard hybrid formulation yields an improvement over the implicit model but still is not able to match the vertical response at hover with sufficient accuracy. The rise in amplitude is not large enough and the amplitude drop occurs at a lower frequency than in the flight test data.

3. EXTENDING THE HYBRID MODEL

3.1 Accounting for Hinge Offset

Because of the deficits in matching the flight test data for the vertical axis in hover, it was tried to improve the hybrid identification model. As the EC 135 with its bearingless rotor has a relatively high equivalent hinge offset of 10%, the influence of hinge offset was investigated first.

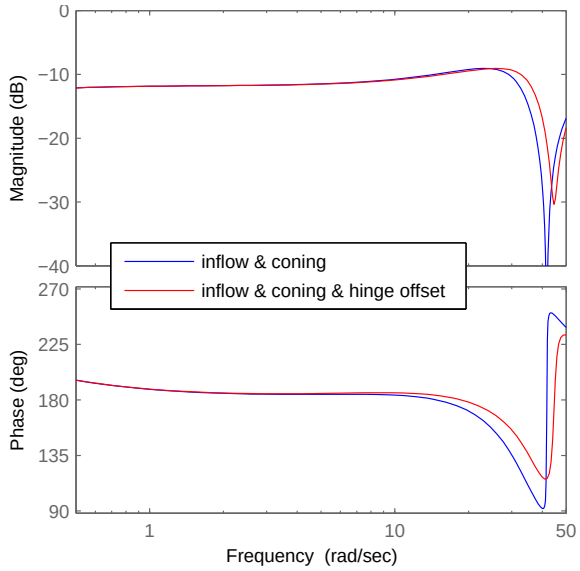

Figure 7: Influence hinge offset on the simulated frequency response for a_z/δ_0 (EC 135 in hover)

Figure 7 shows the difference in the frequency response of vertical acceleration due to collective input with a hinge offset of 10% versus zero hinge offset. It can be seen that the hinge offset moves the amplitude drop to higher frequencies and slightly modifies the phase curve. The influence of hinge offset on the amplitude drop led to the idea that the deficits of the standard hybrid model might partially be caused by ignoring hinge offset. Therefore, the hybrid model was extended accordingly.

According to[4], the coning equation including the influence of hinge offset are:

$$\begin{aligned}\ddot{\beta}_0 = &-\frac{\Omega\gamma}{8}\left(1-\frac{8}{3}\epsilon+\epsilon^2\right)\dot{\beta}_0 \\ &-\Omega^2\left(1+\frac{3\epsilon}{1(1-\epsilon)}+\frac{K_\beta}{I_\beta\Omega^2}\right)\beta_0 \\ &-\frac{\Omega\gamma}{6R}\left(1-\frac{2}{3}\epsilon\right)\nu \\ &+\frac{\Omega^2\gamma}{8}\left(1-\frac{4}{3}\epsilon\right)K_{\theta_0}\delta_{col}\end{aligned} \tag{28}$$

This means that the parameters of the coning equation in (27) have to be changed accordingly. Table 2 illustrates how the numerical values of the derivatives of the coning equation for the EC 135 change when accounting for the 10% hinge offset. The differences between the values with and without hinge offset are on the order of 15-20%.

Derivative	$\epsilon = 0$	$\epsilon = 10\%$
B_{β_0}	-1710	-1970
$B_{\dot{\beta}_0}$	-34.1	-29.2
B_ν	-8.91	-7.08
$B_{\delta_{col}}$	4.26	3.39

Table 2: Influence of hinge offset on coning derivatives (EC 135 values)

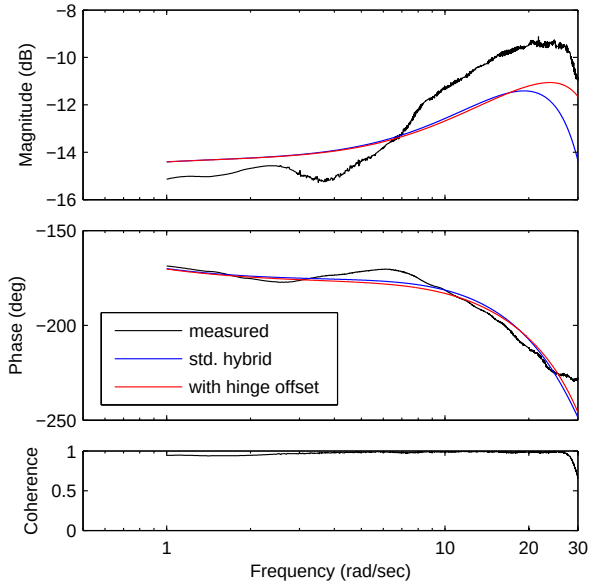

Figure 8: Match in a_z/δ_0 for the hybrid model without and with hinge offset (EC 135 in hover)

Figure 8 shows the improvement when applying the hybrid model that accounts for hinge offset to EC 135 flight test data. It can be seen that the amplitude drop for the vertical acceleration moves to higher frequencies as intended, but the deficit in amplitude raise still remains.

3.2 Freeing Parameters

As the match in vertical acceleration at hover still was not sufficient, additional investigations were performed. In[9] Fletcher applied the hybrid model to UH-60 flight test data and could only achieve an acceptable match by freeing some of the parameters of the hybrid model from their analytical predictions, namely Z_{C_T}, T_ν, $V_{\dot{\beta}_0}$ and V_ν.

Thus, a similar approach was tried for the EC 135. As the identification model from equation (27) does not contain the parameters Z_{C_T}, T_ν, $V_{\dot{\beta}_0}$ and V_ν directly as parameters to be identified, scale factors for these parameters were introduced in the model and estimated.

Derivative	Identified Value	CR bound (%)
Z_w	-0.134	3.6
$\tau_{\delta_{col}}$	0.0234	2.3
f_V_ν	0.920	2.7
f_T_ν	0.717	2.6

Table 3: Identified values of extended hybrid model with Cramer-Rao bounds

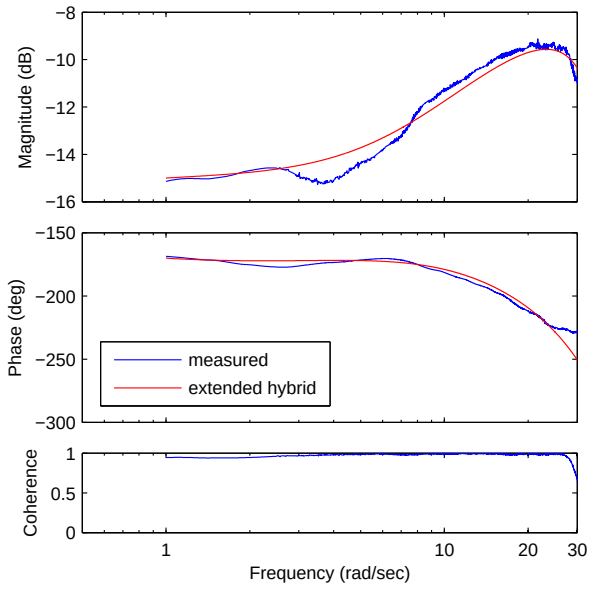

Figure 9: Match of extended hybrid model in hover

Estimating a scale factor for Z_{CT} was not possible because of identifiability problems. Estimating a factor for T_ν gave some improvement and estimating factors for both T_ν and V_ν led to the match shown in figure 9 that is almost perfect. Table 3 gives the corresponding identified values for the parameters of the vertical model together with their uncertainty levels (Cramer-Rao bounds). All model parameters could be determined with high accuracy.

The deviation from the theoretical values is a factor of 0.920 for V_ν. This could be caused by uncertainties in the assumed value of the blade lift coefficient. For T_ν, the deviation is much higher with a factor of 0.717. One possible reason for this deviation is that omitting all coupling to the other axes in the derivation of the hybrid models causes an oversimplification. Incidently, the estimated factors correspond very well to the deviations that were identified by Fletcher for the UH-60 (see[9]).

Table 4 compares the resulting parameters of the vertical model with their theoretical predictions. Note that Z_ν changes from its theoretical values due to the changes in V_ν and T_ν (see equation (23)). The numerical values for the parameters of the coning equation are already listed in table 2.

Derivative	Identified Value	Theoretical Value
V_ν	-15.1	-16.0
$V_{\dot{\beta}_0}$	-35.9	-35.9
$V_{\delta_{col}}$	2.17	2.17
$T_{\dot{\nu}}$	9.74e-5	9.74e-5
T_ν	7.65e-4	0.0011
$T_{\dot{\beta}_0}$	0.0018	0.0018
Z_{CT}	-1.590	-1.590
Z_w	-0.137	—
Z_ν	0.791	1.12
$Z_{\dot{\beta}_0}$	2.69	2.69
$Z_{\delta 0}$	-0.336	-0.336

Table 4: Comparison of identified values and theoretical predictions of the vertical model

After this good match for the hover data had been achieved, the extended vertical model was also applied to the data for the forward flight conditions. The simplified coning equation that is used in the hybrid model is theoretically only applicable to hover data because in forward flight, rotor coning and flapping are coupled via the advance ratio (see[14]). But the coning motion has only a small influence on the overall vertical response in forward flight so that this coupling can be ignored. This could already be seen in figure 4 where the implicit model that neglects coning provides a sufficient match in forward flight.

Therefore, the extended hybrid model was applied without any modification also to the forward flight conditions. No scaling factors for the parameters T_ν and V_ν were necessary for these cases and a good match could be achieved.

4. INCLUSION IN OVERALL MODEL

After the modified hybrid formulation for the vertical axis provided such a good match in the reduced model, it was also implemented in the overall system identification model for the EC 135. This overall model covers the 6-DoF rigid body dynamics and includes an implicit formulation for the regressive flapping that has been shown in[11] to be equivalent to the more common explicit formulation. The regressive lead-lag is modeled by a second-order dipole on the longitudinal and lateral cyclic inputs as described in[1]. Together with the extended vertical model from the preceding section, this leads to a 12-DoF model with 17 states (u, v, w, p, q, r, Θ, Φ for the rigid-body motion, $\dot{p}$, $\dot{q}$ for the implicit flapping formulation, ν, β_0, $\dot{\beta}_0$ for inflow/coning and x_1, x_2, y_1, y_2 for the regressive lag motion).

Engine dynamics have not yet been included in the overall model as the EC 135 engines are controlled by a FADEC (full authority digital engine control) system that keeps engine speed almost constant.

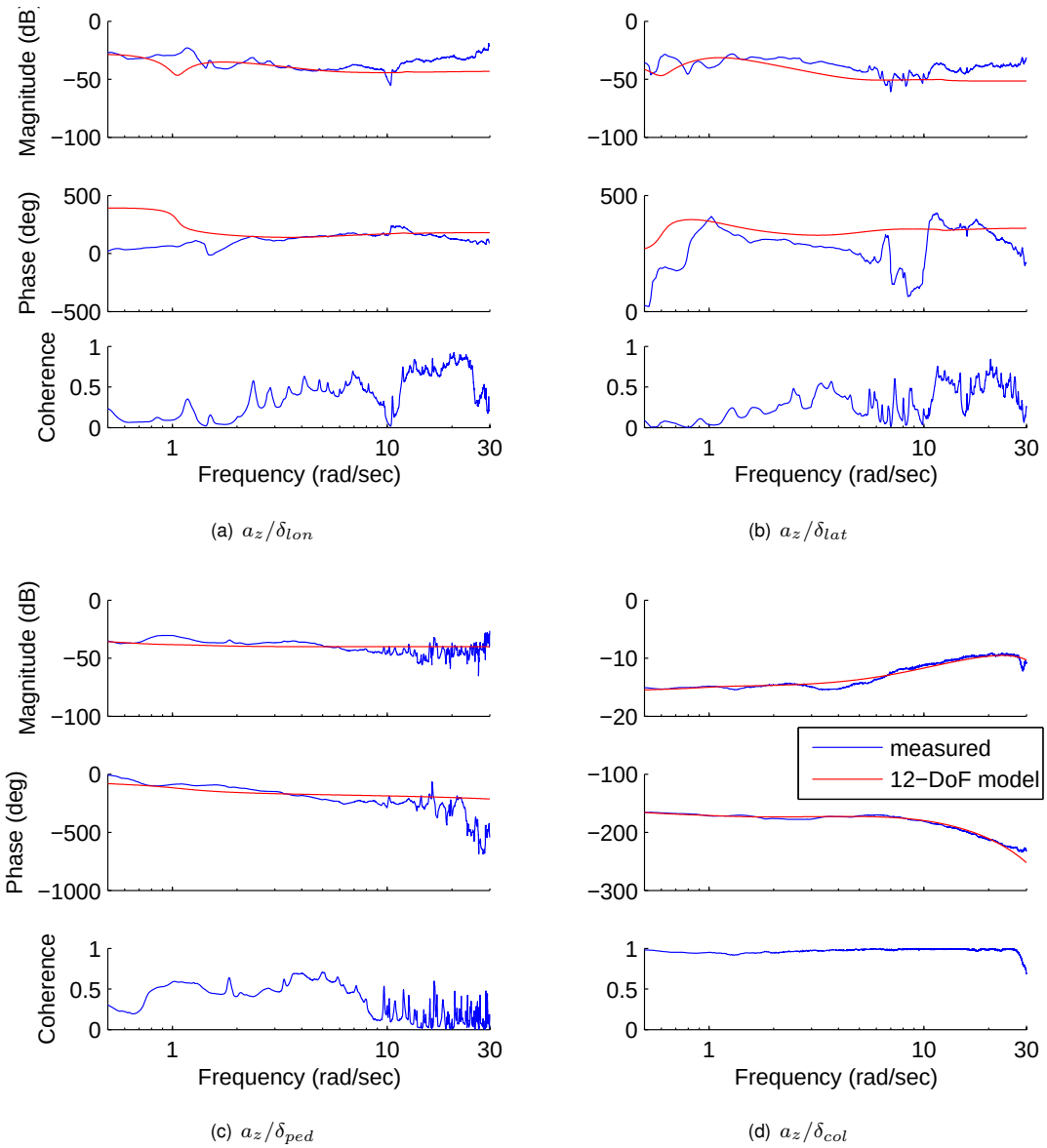

(a) a_z/δ_{lon} (b) a_z/δ_{lat}

(c) a_z/δ_{ped} (d) a_z/δ_{col}

Figure 10: Match in vertical acceleration for the overall model in hover

For the identification with the overall model, the on-axis parameters of the vertical axis were fixed at the values identified with the reduced model because they could not be estimated together with all other unknown derivatives.

By using the extended vertical model also in forward flight, the same model structure could be used for all velocities. Having a single model structure facilitates the interpolation of the identification parameters with airspeed, which is useful for flight-control design at intermediate conditions and for implementation in a continuous full flight envelope simulation[15].

Figure 10 shows the match in vertical acceleration due to all four control inputs for the hover case. It can be seen that the overall model tracks the flight test data very well also for the off-axis responses. The corresponding match for the 60 kts forward flight condition is shown in figure 11.

5. SUMMARY

When modeling the vertical axis of the EC 135, a simple quasi-static model is not sufficient. Therefore, an implicit model was used that models the dynamic inflow and accounts for coning through an equivalent time delay. This implicit model provided sufficient accuracy for forward flight but not for hover.

Thus a standard hybrid formulation accounting for inflow and coning was applied. This led to some improvement but still did not provide a sufficient match for the hover data.

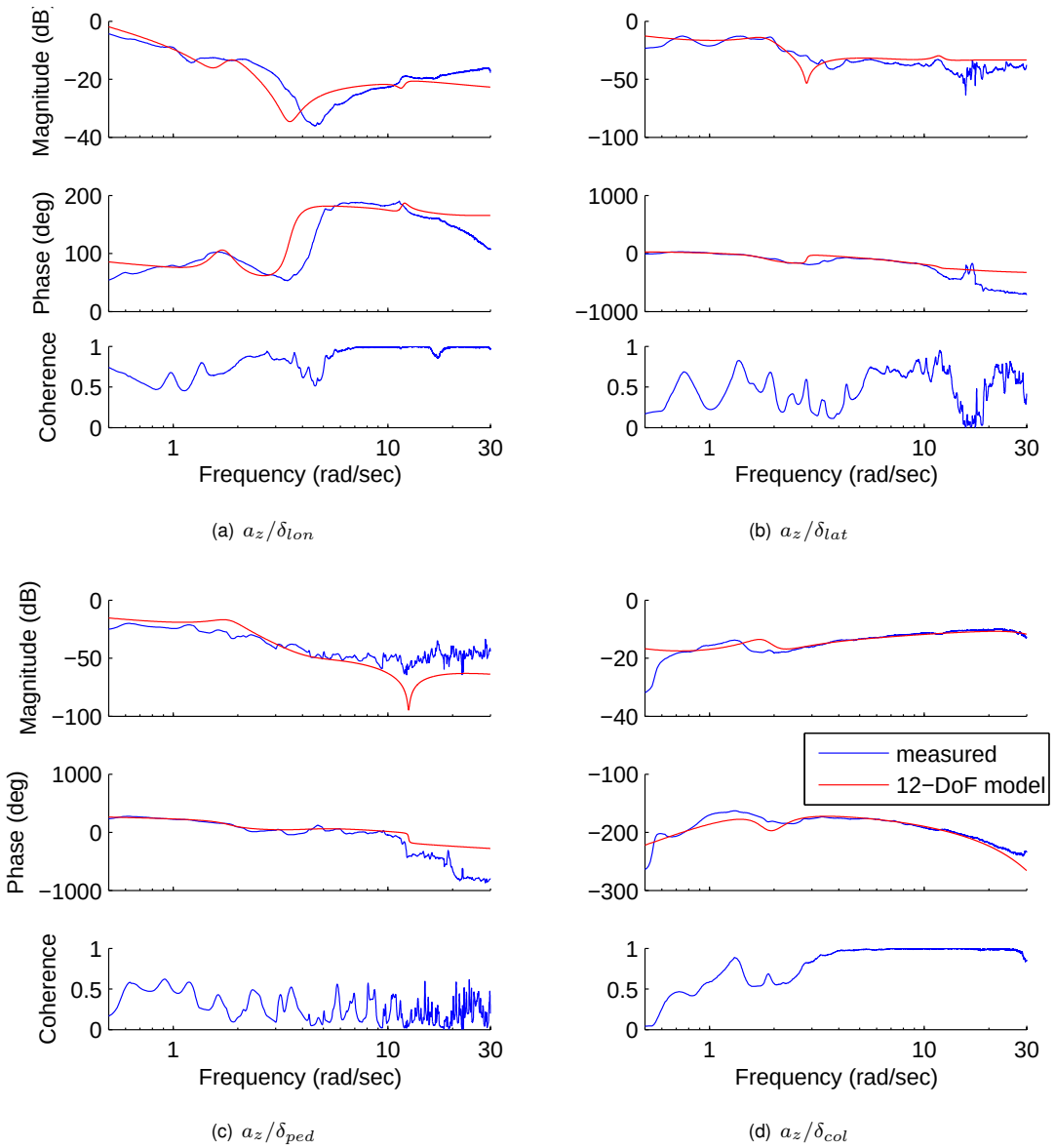

(a) a_z/δ_{lon} (b) a_z/δ_{lat}

(c) a_z/δ_{ped} (d) a_z/δ_{col}

Figure 11: Match in vertical acceleration for the overall model at 60 kts forward flight

Due to the EC 135 having a hinge offset of 10%, the hybrid formulation was extended to account for the hinge offset. Furthermore, two parameters that are usually fixed to theoretical values had to be estimated to match the flight test data. With these modifications, the hybrid formulation provides a good match for the hover case.

This extended hybrid model for the vertical axis was finally used in an overall identification model that includes regressive flapping, inflow/coning and regressive lead-lag and yields a very good match for frequencies up to 30 rad/s.

REFERENCES

[1] Susanne Seher-Weiss and Wolfgang von Grünhagen. EC 135 System Identification for Model Following Control and Turbulence Modeling. In *1st CEAS European Air and Space Conference 2007*, Berlin, Germany, September 2007.

[2] Jeffery A. Schroeder, Mark B. Tischler, Douglas C. Watson, and Michelle M. Eshow. Identification and Simulation Evaluation of a Combat Helicopter in Hover. *Journal of Guidance, Control and Dynamics*, 18(1):31–38, 1995.

[3] Mark B. Tischler and Robert K. Remple. *Aircraft and Rotorcraft System Identification: Engineering Methods with Flight-Test Examples*. American Institute of Aeronautics and Astronautics, Inc., Reston, VA, 2nd edition, 2012.

[4] Robert T.N. Chen and William S. Hindson. Influence of Dynamic Inflow on the Helicopter Vertical Response. Technical Report NASA TM 88327, June 1986.

[5] Mark B. Tischler, Jason D. Colbourne, Jessica L. Jenkins, Luigi S. Cicolani, Kenny K. Cheung, Stuart C. Wright, Anthony C. Acunzo, Naji S. Yakzan, and Vineet Shahsrabudhe. Integrated System Identification and Flight Control optimization in S-92 Handling-Qualities Development. In *AHS 57th Annual Forum*, Washington, DC, May 2001.

[6] Mark B. Tischler and Chris A. Tomashofski. Flight Test Identification of SH-2G Flapped-Rotor Helicopter Flight Mechanics Models. *AHS Journal*, 47(1):18–32, 2002.

[7] Jeff Harding and Scott Moody. Identification of AH-64D Dynamics to support Flight Control System Evaluation. In *AHS 61st Annual Forum*, Grapevine, TX, June 2005.

[8] Chris Quiding, Christina M. Ivler, and Mark B. Tischler. GenHel Model Correlation using Flight Test Identified Models. In *AHS 64th Annual Forum*, Montreal, Canada, May 2008.

[9] Jay W. Fletcher. Identification of a High-Order Linear Model of the UH-60M Helicopter Flight Dynamics in Hover. In *AIAA Atmospheric Flight Mechanics Conference and Exhibit*, Honululu, HI, August 2008.

[10] Jürgen Kaletka, Hermann Kurscheid, and Ulrich Butter. FHS, the New Research Helicopter: Ready for Service. *Aerospace Science and Technology*, 9(5):456–467, 2005.

[11] Susanne Seher-Weiss and Wolfgang von Grünhagen. Comparing Explicit and Implicit Modeling of Rotor Flapping Dynamics for the EC 135. *CEAS Aeronautical Journal*, 2014. DOI 10.1007/s13272-014-0109-0.

[12] P. J. Charpenter and B. Fridovich. Effect of a rapid-pitch increase the thrust and induced-velocity response of a full-scale helicopter rotor. Technical Report NACA TN-3044, 1953.

[13] D. M. Pitt and D. A. Peters. Theoretical prediction of dynamic-inflow derivatives. *Vertica*, 5:21–34, 1981.

[14] Peter D. Talbot, Bruce E. Tinling, William A. Decker, and Robert T.N. Chen. A Mathematical Model of a Single Main Rotor Helicopter for Piloted Simulation. Technical Report NASA TM 84281, September 1982.

[15] Steffen Greiser and Susanne Seher-Weiss. A Contribution to the Development of a Full Flight Envelope Quasi-Nonlinear Helicopter Simulation. *CEAS Aeronautical Journal*, 5:53–66, 2014.

COPYRIGHT STATEMENT